New Materials, Compounds and Applications
Vol.7, No.2, 2023, pp.122-136

RAMAN SPECTROSCOPY AND STRUCTURAL CHARACTERISTICS OF FLUORESCEIN AND COUMARIN DOPED SILICA SOL, GEL, AND AEROGEL

Mohammed A. Anaad[1], Israa F. Al-Sharuee[2*]

[1]Department of Physics, College of Science, Al-Anbar University, Al-Anbar, Iraq
[2]Department of Physics, College of Science, Mustansiriyah University, Baghdad, Iraq

Abstract. In this study the aerogel is obtained, doped with of dye laser coumarin and fluorescein on the molecular structure of silica aerogel prepared by easily scalable sol-gel dripping methods and then dried to aerogels. The effect of the drying techniques and heat-treated temperature the superhydrophobic silica aerogel and the alcogel was further obtained by alcoholization of the hydrogel. The surface of alcogel was modified by reacting with trimethylchlorosilane (TMCS) diluted in n-hexane. In addition, silica aerogel exhibited excellent physical, morphological, microstructural and chemical properties. The development of the compositional profiles within the sol, gel, and aerogel was discussed in order to examine the spectral properties of fluorescence and absorption. Fourier Transform Infrared Spectroscopy (FTIR) was used to examine this effect, in addition to Field Emission Scanning Electron Microscopy (FESEM), and surface area measurement. It was found out from FTIR data that the dye laser keeps the inner structure of samples. Results show more difference in peak regions and distribution in Raman spectrum in case of sol, gel and aerogel samples, besides the homogenies and nano-structure are domine.

Keywords: *Fluorescein and Coumarin, Doped aerogel, Raman spectrum, Silica gel.*

Corresponding Author: *Israa F. Al-Sharuee, Department of Physics, College of Science, Mustansiriyah University, Baghdad, Iraq, Tel.+964 7702787336, e-mail: i81f54@uomustansiriyah.edu.iq*

Received: *27 May 2023;* ***Accepted:*** *27 June 2023;* ***Published:*** *4 August 2023.*

1. Introduction

Sol-gel is one of the most successful techniques to fabricate high photocatalytic Alumina nanostructures (Wang *et al.*, 1999). Some heterogeneous material qualities, such as the necessary porosity, optical permeability, and chemical stability are studied (Martinelli, 2014).

The method known as "sol-gel" entails creating an amorphous gel from a precursor solution. Metal alkoxides are frequently used as the starting material in this molecular precursor-based approach. Better uniformity and purity from the raw materials, lower preparation temperatures that conserve energy, and the capacity to create novel compositions are some benefits of the sol-gel process (Depla *et al.*, 2011). Physical gels are often created utilizing reversible interactions, but covalently bonded hydrogels are more durable materials that can withstand repeated swelling and shrinking without losing their mechanical properties. To produce silica-based materials relevant for several different applications, sol-gel synthesis is a crucial chemical process because of its comparatively inexpensive processing costs and controllable grain size (Yun *et al.*, 2014;

How to cite (APA):
Anaad, M.A., Al-Sharuee, I.F. (2023). Raman spectroscopy and structural characteristics of fluorescein and coumarin doped silica sol, gel, and aerogel. *New Materials, Compounds and Applications*, *7*(2), 122-136.

Zhang *et al.,* 2012). Silica aerogel is a material renowned for its strong mechanical and thermal characteristics, which may be particularly beneficial in a variety of applications. Little focus has been placed on its optical qualities, however, since it is not transparent to light (Al-Mothafer *et al.,* 2021) for the same reason, random laser systems may be housed in low-density silica aerogel. Combining the above-mentioned benefits of random lasers with a stable and light matrix might be useful in various applications, notably those involving the outer space. In addition to being useful as an optical limiter and in high power lasers, SA's high nonlinear optical coefficient (comparable to that of glass) and minimal optical nonlinear absorption make it a promising candidate for other uses as well (Braidotti *et al.,* 2016). Due to its high loading capacity, outstanding adsorption capabilities, and high biocompatibility, silica aerogel is a potential nano-porous material for drug delivery systems (Mohammadian *et al.,* 2018; Stergar & Maver, 2016). The technique of making silica aerogel is well-developed, and it may be used for specific purposes by changing the parameters of its synthetic production (Du *et al.,* 2013). Many researchers have explored how doping and adding catalysis to silica aerogel might enhance its morphological and structural features by using techniques including Raman spectroscopy, Fourier transform infrared spectroscopy, and atomic force microscopy. This is done before the gel is dried, obtain a polymer coating on the silica aerogel's surface, which greatly increased the material's durability against cracking. The easiest method to improve the strength of silica aerogel is the employment of fiber reinforcing techniques. Incorporating short fibers into the silica aerogel structure, either randomly or as an extended mat, serves primarily to support the structure. Despite their impressive structural properties and modest compressive strength, silica aerogels are very brittle (Tang *et al.,* 2017). In Lovskaya et al. (2015) the results indicated that the release rate for several medicinal components increased. As comparison to pure active pharmaceuticals, it took less time for drug-loaded aerogels to release and dissolve 50% of the active ingredient. The main in-vivo tests were conducted to compare the aerogel-loaded active ingredient's bioavailability to that of the pure active medication. The results demonstrated that drug-loaded samples had greater bioavailability values than did pure active medicines. The results obtained in Al-Sharuee and Ali (2023) demonstrated that the molar electronic transition energy rose with a reduction in the maximum absorption wavelength, with acetone solvent having the highest intensity of the absorption spectrum. In addition, the “C=O” band, “O=C-O, C-C” and “C-O deformation are responsible for a number of bands in the Raman shift. The stretching and bending modes of the “O-H” and “C-O” components make up the “O-H” group's distinctive vibrations.

The morphologies, pore size distributions, and chemical structure of two precursors' effects on the sponge-reinforced silica aerogels (Li *et al*., 2018). Cheng *et al.,* 2016 showed that the ambient pressure drying might cause reversible shrinkage in the silica gel modified using TMCS, which kept the mesoporous structure lower density, and high specific surface area. Granules of water-based aerogel were made without using organic solvents and to complete the full procedure dried at a room temperature during 6 hours. The produced silica aerogel has a consistent mesoporous structure and a low thermal conductivity (0.0237-0.0245 W/mK^{-1}) (Huang *et al.,* 2019). In Al-Sharuee (2021) is doped with dye laser to raise the contact angle, through that the Cl in the dye structure interact with -OH, which prevents H from joining with -OH and causing the aerogel's humidity. Moreover, the found doping gave the product more homogeneous structure and transparency. Mohammadian et al. (2018) increased number of non-bridging oxygens in the gel structure caused by greater Na/Si ratios, and reduced the degree of cross-linking.

One of the interesting technique to learn the effect of the alkalis to the gel's structure is Raman spectroscopy. Al-Sharuee (2021) indicates that heating impacted in a decrease in density, which produced more insulating metal. Moreover, varying pH has a significant influence on thermal conductivity. In Quino et al. (2016) aerogels in ambient pressure are prepared and the Raman and fluorescence and absorption spectrum are investigated in different cases as sol, gel, and aerogel.

2. Experimental procedure

Tetraethylorthosilicat (98 %) from Sigma-Aldrich, Germany. Trimethylchlorosilane (98%) TCI Japan. Hexane (> 98%), from CHem-LAB (Belgium). Ethanol from Schariau (Spain) > (99%) Hydrochloric acid (35-38%), from Thoma Baker (India). Ammonia Solution from CDH (India). Prepare the silica (sol, gel, modified gel, and aerogel doped with laser dyes in (10^{-2}) gm/cm ^{3}, and dissolved dyes fluorescein add (0.166g) and coumarin (0.073g) in(50ml) ethanol. Molecular weight of coumarin (146.145g/ml) and chemical formula $C_6H_6O_2$ molecular weight of fluorescein (332.31g/ml) and chemical formula $C_{20}H_{12}O_5$

Condensed silica (CS) was created in the first stage by mixing TEOS as a precursor in ethanol at a molar ratio of 20MI with 40ml of ethanol and stirring on a magnetic stirrer for 10 minutes. Then, 2ml of HCL [0.1M] was added as an acidic catalyst. Before adding the base catalysis (0.5M NH_4OH) to turn the sol into a gel, the preparation stage sol (5ml) of fluorescein and coumarin was combined with (10ml) of condensed. Each was then placed under a magnetic stirrer for 15 minutes. The gel is aged for two hours after 15 minutes, and it is then cleaned in ethanol three times every 24 hours. By combining TMCS (7.5ml) and (30ml) hexane, a surface modification was created and applied to the gel that had was oven at 60°C for 24 hours. Then exchanged with pure hexane at room temperature and was washed in pure hexane and covered the holder in selofin with tiny holes and the gel was dried at room temperature in the oven at temperatures up about (180℃) gradually every 20 ℃.

3. Method of characterization

By examining the infrared absorption spectrum, it can be provided information about the molecules that are present in a sample. Fluorescence spectroscopy uses a beam of light that excites the electrons in molecules of certain compounds, and causes them to emit light. The measurement of molecular vibrations and phonons by Raman spectroscopy yields detailed knowledge on the chemical makeup, molecular conformation, and chemical structure of the sample. FTIR is a subfield of spectroscopy that focuses on the infrared portion of the electromagnetic spectrum describes the degree of surface roughness, the examination of particle size, and surface topography characteristics. AFMs are atomic force microscopes, which are among the contemporary technologies. The topography of surfaces with nano- and micro-dimensions can also be known by field emission scanning electron microscopy (FESEM).

4. Results and discussion

Figs. 1 and 2 shows the UV absorption of coumarins in ethanol whereas the absorption spectrum is closely related to the arrangement of energy levels. The maximum

absorbance peak was discovered in the sol phase at 470nm, followed by the addition of NH_3OH, and subsequently it converted into the gel. It detects a change in the absorbance value, and the highest value is at the wavelength of 460nm. The short positivity, i.e., high energies, is high in the ultraviolet region and decreases in the visible regions. This is explained by the fact that the falling photon does not have enough energy to interact with the atoms. In the case of high wavelengths, the photon will move, meaning there will be an interaction between the fallen photon and matter. The absorbance was determined in the sol phase and the fluorescein grafted gel phase using two figures. The maximum absorbance peak was detected in the sol phase at 280nm, and then it was changed into the gel by the addition of NH_3OH. It notices a shift in the absorbance value, with the maximum value at 290nm. The brief positivity i.e. high energies, is greatest in the ultraviolet area and declines in the visible range (Al-Sharuee & Ali, 2023).

Absorption analysis

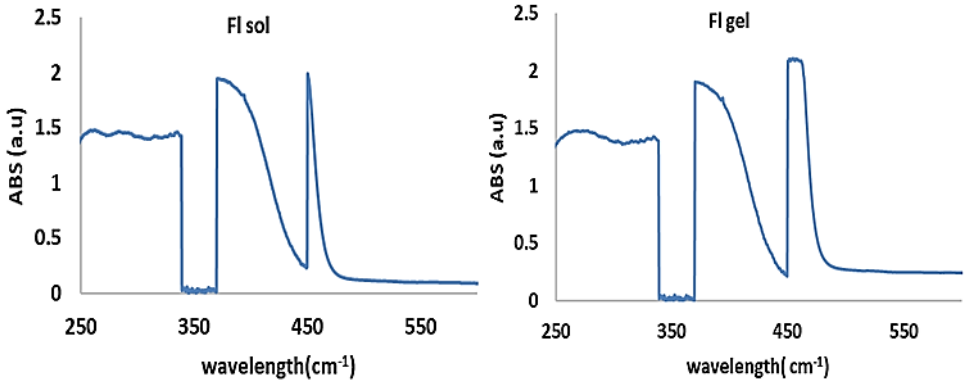

Fig. 1. Absorption spectrum for doped silica (a):sol, (b): gel with fluorescein

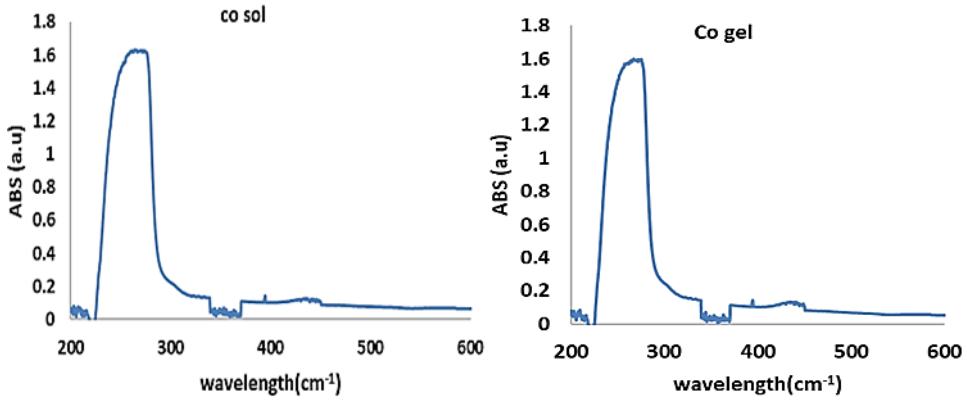

Fig. 2. Absorption spectrum for doped silica (a): sol, (b): gel with coumarin

Fluorescence analysis

The slight shift in the peak of the fluorescence spectrum is attributed to the difference in particle size the results showed a clear peak in the wavelength560nm range in the sol phase, and more than one clear peak after transition to a gel, because the gel is denser than the sol phase and the highest peak in the wavelength range 590nm. An

application of fluorescence spectrometry is to determine the crystal structure of the surfaces of materials was used Photoluminesces fluorescence Photoluminescence is a physical phenomenon used to investigate the electronic structure of matter.

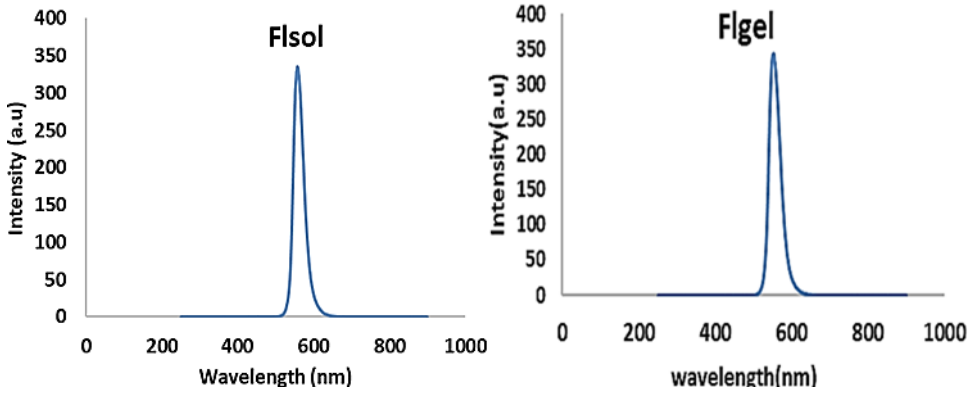

Fig. 3. Fluorescence spectrum for doped silica (a): sol, (b): gel with fluorescein

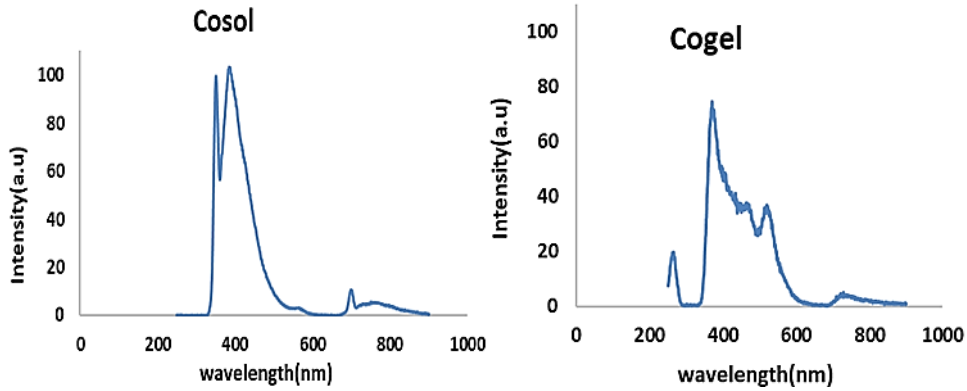

Fig. 4. Fluorescence spectrum for doped silica (a): sol, (b): gel and coumarin

As it seen from the figure for the sol-gel coumarin dye solution, the fluorescence intensity has a maximum value of at a wavelength of 380nm nanometers the after transfer to a higher density gel it becomes more active. It can be seen that the fluorescence intensity in peak in the wavelength range 390nm the case of silica gel doped with fluorescent nanoparticles is more intense than in case sol. This can be attributed to the unconstrained random motion of the liquid particles which is larger than that of the solid particles. This results in energy dissipation due to particle collision indicating that the expansion mechanism is homogeneous in type. Since the distance between molecules in a solid is small, collisions between molecules are very rare, and therefore no significant energy loss is observed. It can be seen that the fluorescence intensity in the case of silica gel doped with fluorescent nanoparticles is more intense than in case sol. This can be attributed to the unconstrained random motion of the liquid particles which is larger than that of the solid particles. This results in energy dissipation due to particle collision indicating that the expansion mechanism is homogeneous type. Since the distance between molecules in a solid is small, collisions between molecules are very rare, and therefore no significant energy loss is observed (Jathar *et al.,* 2021).

Raman analysis

The Raman spectrum for sol, gel and aerogel samples doped with fluorescein and coumarin dyes are shown in Figures 5 and 6, as well tables 1 and 2 illustrated the vibrational modes and the peaks region in the charts.

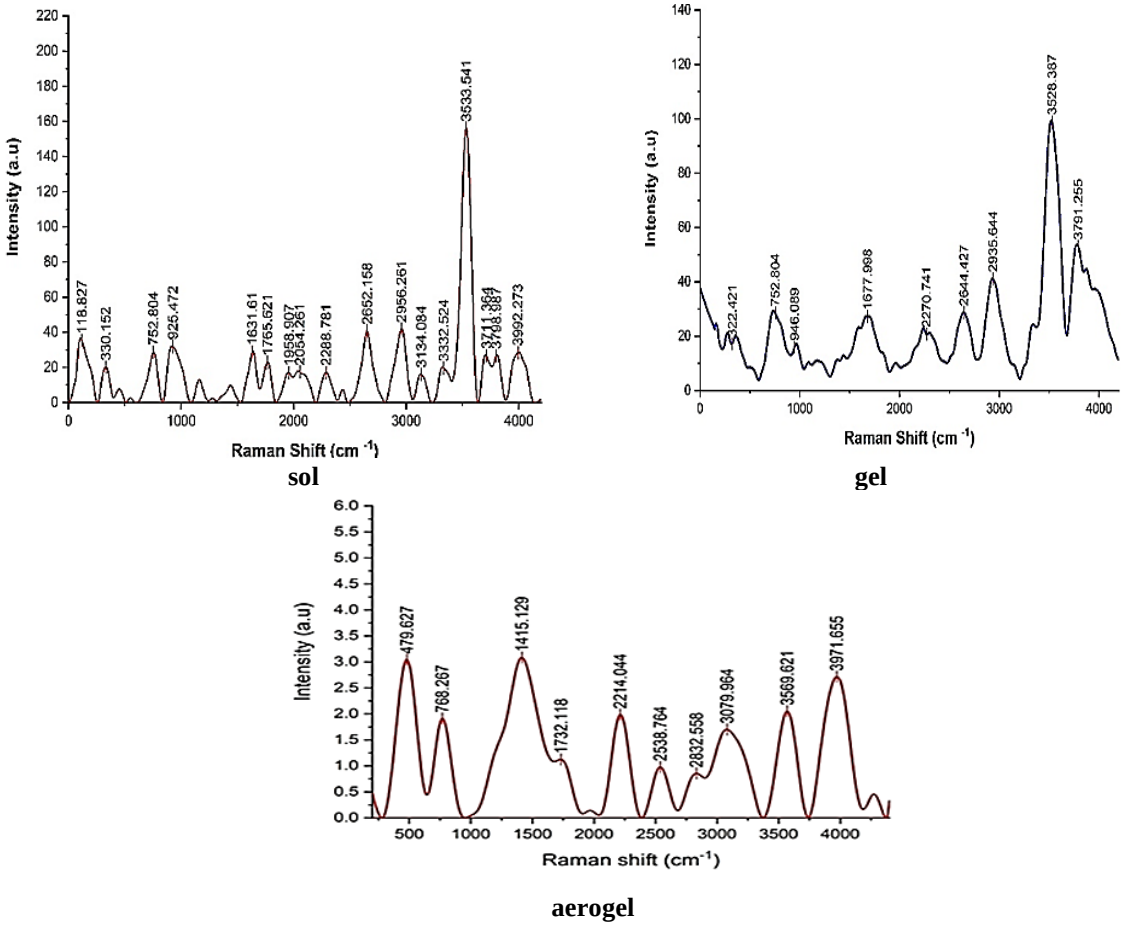

Fig.5. Raman spectrum of doped silica sol, gel, and aerogel fluorescein

Table 1. The main peaks of fluorescein Raman and vibration modes (Rzhevskii, 2021)

Sol doped with fluorescein					
X(cm^{-1})	**band**	**Y (a.u)**	**X(cm^{-1})**	**band**	**Y (a.u)**
118.827		35.19958	2652.158	(S-H)	40.57562
330.152	(C - C)	20.09248	2956.261	(C-H)	41.82074
752.804	(C - S)	28.60832	3134.084	(C-H)	15.99088
925.472	(ClO_3)	32.07938	3332.524	(N-H)	19.69301
1631.61	(C=N)	28.68937	3533.541	(O-H) in liquid	155.9881
1765.621	(C=O)	22.80944	3711.364	(O-H) in solid	26.65564
1958.907	(N=C=N)	16.90007	3798.987		26.55126
2054.261	(SCN)	17.40186	3992.273	(H_2)	28.45699
2288.781	(C≡C)	17.1047			

Gel doped with fluorescein					
x (cm^{-1})	**band**	**Y (a.u)**	x (cm^{-1})	**band**	**Y (a.u)**
322.421	(C - C)	17.20761	2644.427	(S-H)	28.70942
752.804	(C - S)	28.4633	2935.644	(CH_2)	41.12036
946.089	(ClO_4)	15.8961	3528.387	(O-H)	98.8997
1677.998	(C=N)	27.23291	3791.255	(O-H) in solid	52.96177
2270.741	(C≡C)	20.72162			
Aerogel doped with fluorescein					
X (cm^{-1})	**band**	**Y (a.u)**	X (cm^{-1})	**band**	**Y (a.u)**
479.627	(Si-O-Si)	3.0478	2538.764	(S-H)	0.97973
768.267	(C-S)	1.913	2832.558	(CH_2)	0.85717
1415.129	(CH_3)	3.0842	3079.964	(C-H)	1.7009
1732.118	(C=O)	1.126	3569.621	(O-H)	2.0511
2214.044	(P-H)	1.9887	3971.655	(H_2)	2.7151

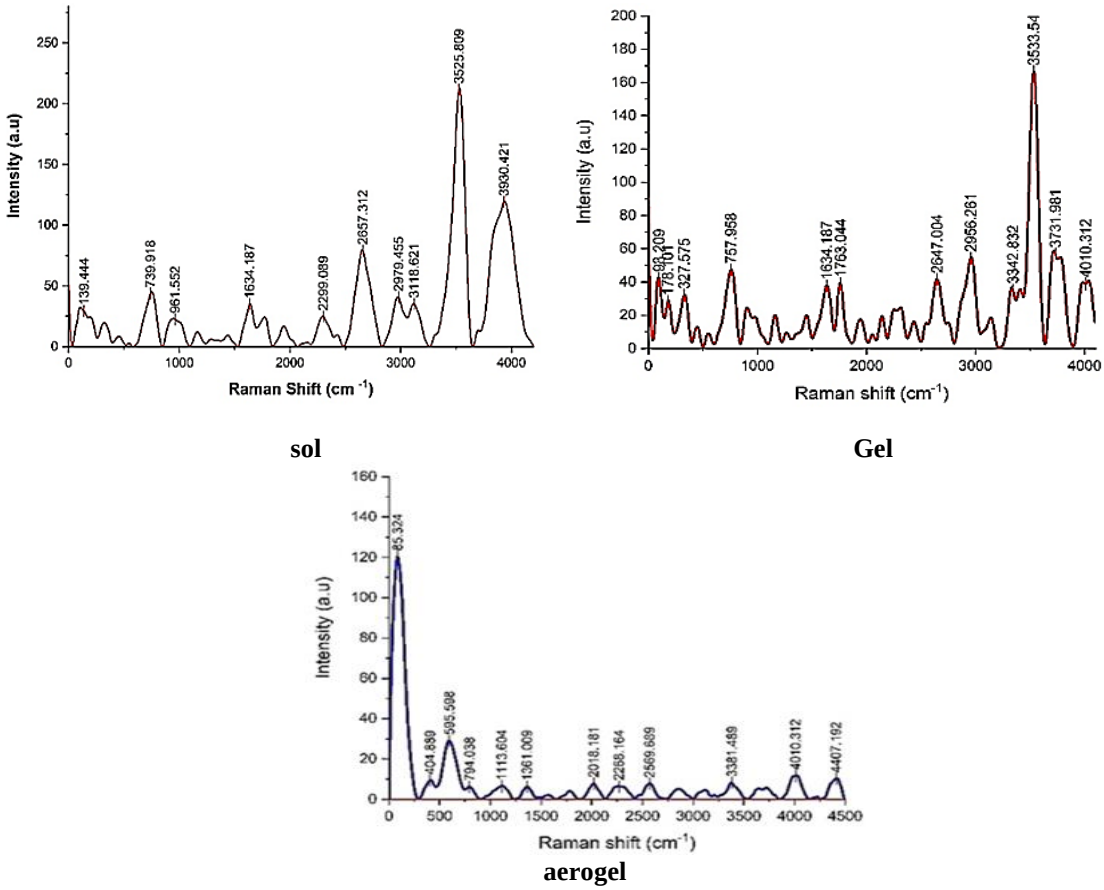

Fig. 6. Raman spectrum of doped silica sol, gel, and aerogel coumarin

Table 2. The main peaks of coumarin Raman and vibration modes(Rzhevskii, 2021)

Sol doped with coumarin					
X (cm^{-1})	**band**	**Y (a.u)**	**X (cm^{-1})**	**band**	**Y (a.u)**
139.444		29.363	2657.312	(S-H)	79.187
739.918	(C-S)	43.825	2979.455	(C-H)	40.761
961.552	(SO_3)	22.664	3118.621	(O-H)	35.284
1634.187	(NH_2)	34.805	3525.809	(O-H)	211.75
2299.089	(C≡C)	24.88	3930.421	(H_2)	119.12
gel doped with coumarin					
X (cm^{-1})	**band**	**Y (a.u)**	**X (cm^{-1})**	**band**	**Y (a.u)**
98.209		41.58	2647.004	(S-H)	42.191
178.101		54.409	2956.261	(C-H)	28.26
327.575	(C-C)	35.08	3342.832	(N-H)	31.907
757.958	(C-S)	166.46	3533.541	(O-H) in liquid	47.263
1634.187	(NH_2)	56.888	3731.981	(O-H) in solid	37.647
1763.044	(C=O)	38.925	4010.312	(H_2)	39.048
Aerogel doped with coumarin					
X (cm^{-1})	**band**	**Y (a.u)**	**X (cm^{-1})**	**band**	**Y (a.u)**
85.324		120.24	2018.181	(N=S=C)	7.8463
404.889	(S-S)	9.4384	2268.164	(C≡C))	6.3412
595.598	(C-Br)	28.944	2569.689	(S-H)	7.7336
794.038	(C-F)	6.1615	3381.489	(N-H)	8.1463
1113.604	(C-S)	6.42	4010.312		11.671
1361.009	(C-N)	6.2368	4407.192	(H_2)	10.255

The Raman spectra for each of the sol-phase reactants were collected. The highest intensities are at wavelength 3525.809 and 3930.421nm. The presence of TEOS functional groups leads to similarly located Raman domains. This includes the Si−O expansion mode of the silicon oxide located in the region 690.952. As can be seen, the silicon oxide molecules have a strong Raman peak in the region 353.54-3731.918 cm-1 which corresponds to the stretching vibration of the Si OCxH2x + 1 bond where the oxygen atom is attached to an alkyl group (Kottsov *et al.,* 2023). The stronger Raman intensity of this peak relative to TEOS is attributed to the higher polarizability of the SiO bonds in the methyl-based precursor. In general, it is possible to distinguish the major regions in the Raman spectroscopy of fluorescein-doped aerogel (Ramirez *et al*., 2021). Note a shift in the Raman spectroscopy that appeared in the highest intensity appeared at the wavelength 85.324.-595.598 nm for the aerogel prepared by surface modification using TMCS/hexane. This is due to the single type vibration represented by the symmetric stretching vibration. While for the lowest intensity peaks appeared at the next wavelength 3630.433-4330.878nm the appearance of these peaks of lower intensity is due to the symmetrical expansion vibration of two types of atoms. As for coumarin, there are clear differences in the intensity of fluorescein from the figures. In the initially, Raman spectra

were obtained for each stage of the samples (Depla *et al.*, 2011). The highest intensity at Raman wavelength of the sol phase was 3525.809–3930.421 nm. The presence of TEOS functional groups leads to symmetric Raman domains. After that, the sol-gel process was performed, and the highest intensity was at the wavelengths 3533.54 - 3731.981 nm, and we notice that there are differences in the characteristic Raman intensities of the main components in the mixture. This includes the Si−O expansion mode of the existing silicon oxide. Silicon oxide particles have a strong Raman peak in the region 757.958 nm which is consistent with the stretching vibration of the. it is possible to distinguish major regions in the Raman spectroscopy of coumarin-doped aerosol gels. We notice a change in the Raman spectroscopy. The highest intensity peaks appeared at the wavelength 85.324-595.598 nm for the antenna gel prepared by surface modification using TMCS/hexane. This is due to the single type vibration represented by the symmetric stretching vibration while for the lowest intensity peaks appeared at the next wavelength 3630.433-4330.878nm. The appearance of these peaks of lower intensity is due to the symmetrical expansion vibration of two types of atoms (Quino *et al*., 2016).

FTIR analysis

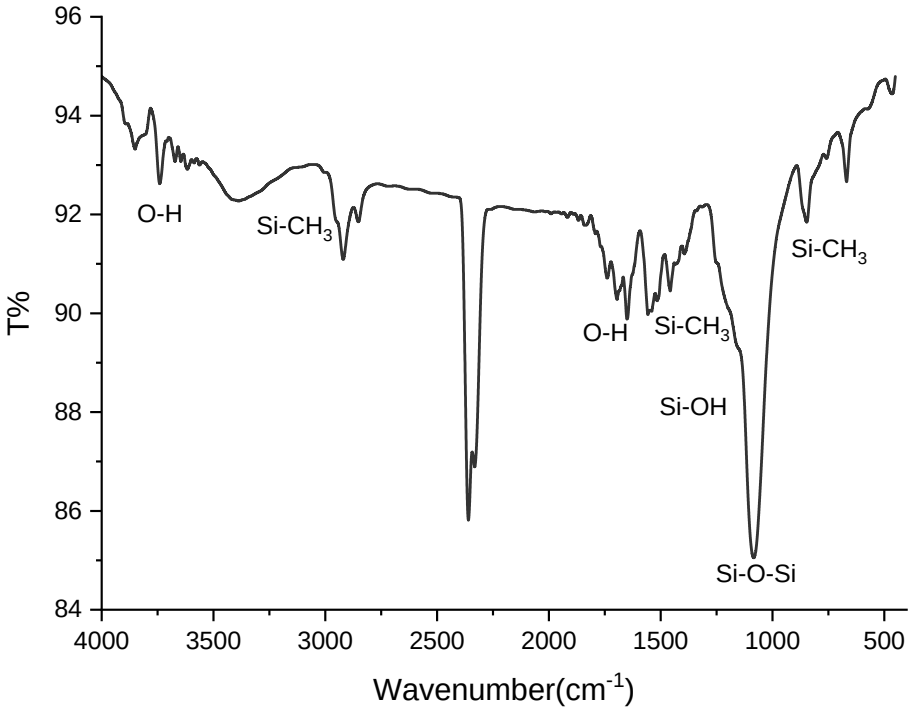

Fig. 7. FTIR spectrum of doped silica aerogel with fluorescein

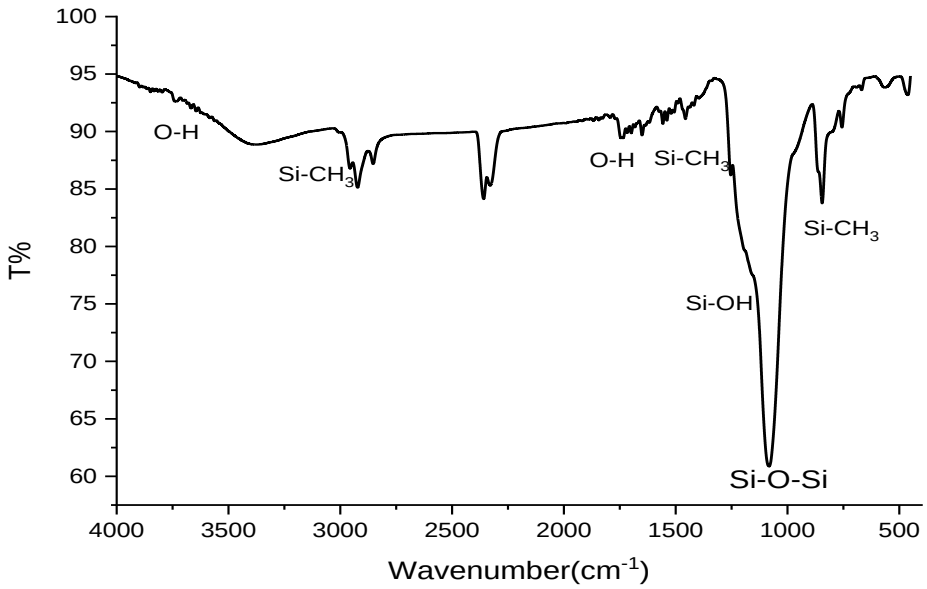

Fig. 8. FTIR spectrum of doped silica aerogel with coumarin

Figs. 7 and 8 present the FTIR-spectrum for sol, gel and aerogel doped with fluorescein and coumarin. In all samples, there are noticeable strong peaks at 2359 cm^{-1} and 1083 cm^{-1} due to Si–O–Si bands, this trough becomes less visible (Al-Husseny *et al*., 2022). The bending stretching of Si-CH_3 was seen in the peaks at 3383 cm^{-1}, 1548 cm^{-1}, and 848 cm^{-1}. At the same time, the peaks assigned to the H-OH lie at 3671 cm^{-1} and 1695 cm^{-1}. Furthermore, the peak attributed to the Si-OH at 1160 cm^{-1} is significantly reduced with the subsequent alteration of TMCS/n-hexane, as shown in the figures (Al-sharuee, 2019). Because of the high effect of a modified solution, the hydrophobic groups (alkyl) replaced the hydrophilic ones (silanol groups). Also, this peak becomes stronger when, as shown in the figure, leading to the success of the modification of TMCS/n-hexane, and surface modification was almost completed. Other peaks were observed at 3671 cm^{-1} and 1695cm^{-1} and were attributed to H-OH bands which were much reduced, to the point that the Si-OH 1160 cm^{-1} peak was no longer noticeable (Sarawade *et al*., 2010). As for coumarin, when the rays shine on the molecule, it vibrates within certain patterns that depend on the nature of the molecule. The model that contains silica, the spectrum appears in the region of there are noticeable strong peaks at 1082 cm^{-1}, and845cm^{-1} due to Si–O–Si bands, this trough becomes less visible. The bending stretching of Si-CH_3 was seen in the peaks at 3369 cm^{-1}, 1520 cm^{-1}, and 845 cm^{-1}. At the same time, the peaks assigned to the H-OH lie at 3644 cm^{-1} and 1650 cm^{-1}. Furthermore, the peak attributed to the Si-OH at 1160 cm^{-1} nanometers, and the sample that contains hydroxide OH will show a peak at 3400 cm^{-1} nanometers and it will be small for the hydrophobic substance. After modifying the surface of the sample by adding TMCS / hexane, new peaks will be generated for us that belong to the silanol group, which has been replaced by the hydroxide group, and it will appear in a region close to the Si–O–Si region (Berardi & Zaidi, 2019).

(AFM) Atomic Force Microscope

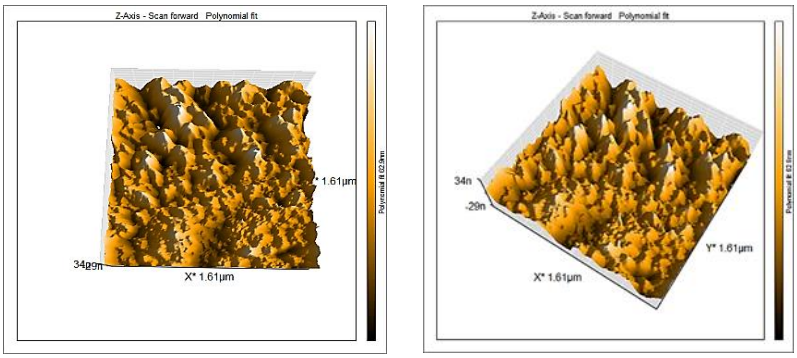

Fig. 9. AFM images of doped silica aerogel with fluorescein in different nanoscale

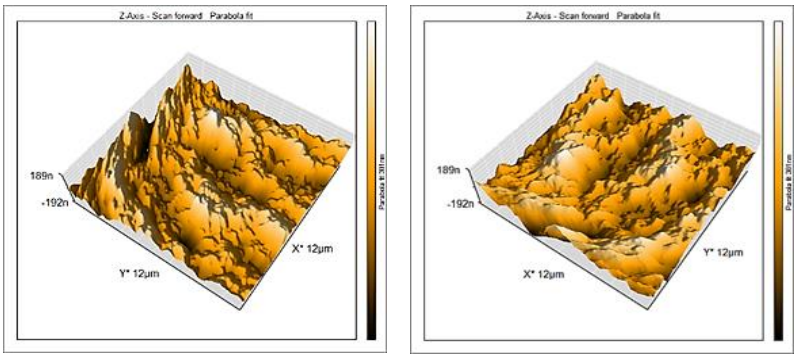

Fig. 10. AFM images of doped silica aerogel with coumarin in different nanoscale

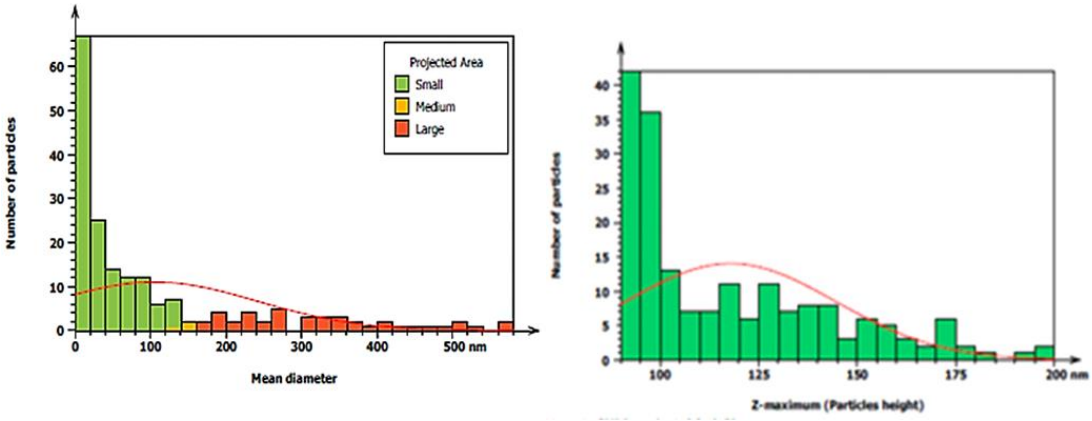

AFM images of doped silica aerogel with fluorescein

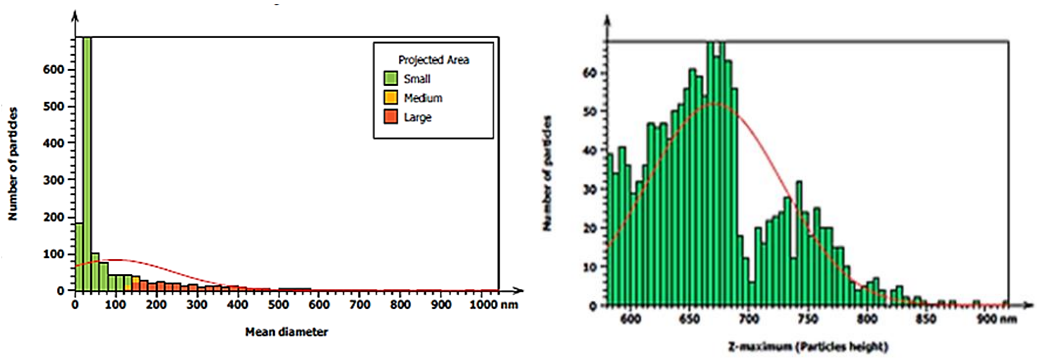

AFM images of doped silica aerogel with coumarin

The atomic force microscope (AFM) for sol, gel and aerogel doped with fluorescein and coumarin is given in this figure. The surface's topography consists of a roughened surface with morphologies resembling nanopillars that come in a variety of sizes and shapes. The distribution of the hotspots, or nano peak-peaks, throughout the surface is uniform and they have generated in a certain way. The important factors of the rough surface analysis, peak-peak, depth of the core-roughness, and density of the summits. Just the grain size on the sample surface is measured by the AFM analysis. The crystal comprises of two grains in the same direction and separated by grain borders might be explained by the fact that the grain includes multiple crystals that are oriented in the same direction. The surface's vertical and horizontal dimensions provide a detailed description of the nanostructure shape. The roughness squared is represented by the root. The surface roughness factor is critical since it indicates surface quality and growth legumes. The quantity of nanoparticle growth is represented by the maximum height. The horizontal dimensions of the surface were estimated using three-dimensional (3D) pictures of the entire surface topography, and the nanoparticles' enhanced surface area endowed them with unique features. The aerogel is grafted with coumarin. The atomic force microscope (AFM) To study the surface topography of nanoparticles in conditions of preparation on it because it has the ability to form microscopic images and examine the surface of samples to provide maximum accuracy. Valuable statistical values for average grain size and in addition to providing important information. The grain size is measured on the surface of the sample. We note in the two figures the maximum height of the bumps for the surface roughness and the number of particle sizes, and the objects are either large is approximately 137.8 nm medium or small, and the highest particle value is 119.4nm.

FE-Scanning Electron Microscopy

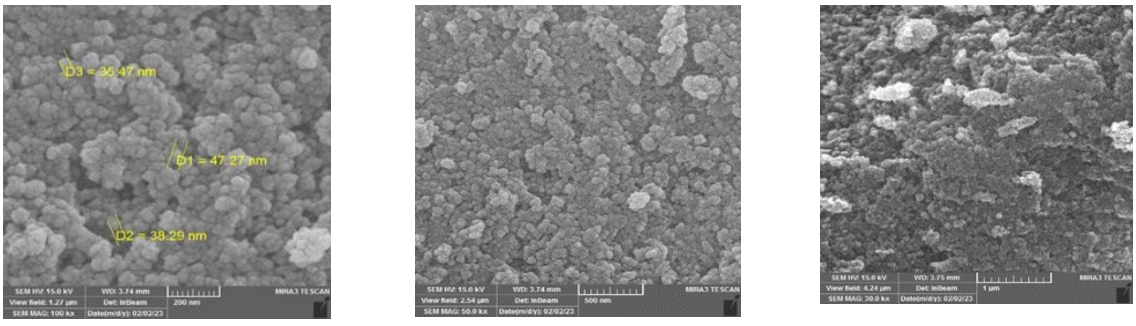

Fig.11. FESEM images of doped silica aerogel with fluorescein in different magnification

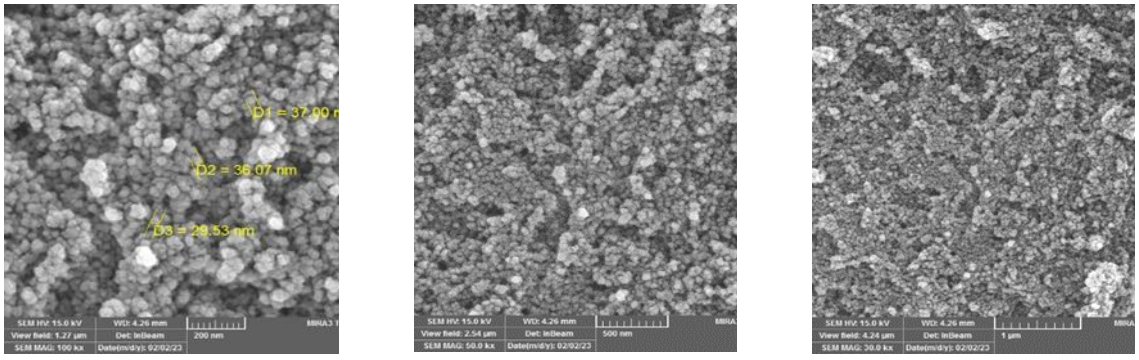

Fig. 12. FESEM images of doped silica aerogel with coumarin in different magnification

The microstructure of silica aerogel was captured by SEM for fluorescein in (Fig. 11). The samples have a typical nonporous structure, and the structural particles are loose and distributed. From the SEM images, it is inferred that the morphology of our samples is dominated by the latter structure. The high depth-of-field feature imaging feature is measured by the chemical composition of the surface features. From FESEM clear tiny pore size, along with the fact that the silica aerogel seems to be a continuous and densely cross-linked network, results in an extremely open structure in which individual particles are not distinguishable and the average particle size is rather large. By using a field emission scanning electron microscope, we were able to see the microstructure of the material (FESEM). The silica aerogel appears in clusters and when clustered together, the particles are aggregations too, and the surface shape is smooth. Moreover, there was microstructural inhomogeneity, and the average particle The image of showed the microstructure by field emission scanning electron microscope (FESEM) and in using FESEM at various magnifications, the coumarin morphological characteristics of the aerogel samples with doping for of were characterized. According to (Fig.12), the particles were aggregated into sphere-shaped aggregates with a typical tridimensional disordered porous structure diameter of around 37.00 nm. All silica aerogel samples feature a three-dimensional network made up of nanometer-sized silica particles that resembles a string of pearls or tiny balls, which was formed during the alcohothermal reduction while the porous structure was preserved. Using the Image application, the grain diameters and the grain diameter average were discovered. One of the things that affects the surface morphology is surface flaws (Falsafi *et al*., 2020).

5. Conclusion

To summarize, nanoparticles were produced and doped by utilizing the sol-gel-aerogel approach. The AFM method was used to analyze the morphology of these particles. In the case of high wavelengths, the photon will move, implying that the fallen photon will contact with matter. Fluorescence and the influence of these have revealed a greater difference in peaks areas and distribution in the Raman spectrum in the case of sol, gel, and aerogel samples, where homogenies and nano-structure are dominant. There was also microstructural variability, and the mean particle size was considerably different from the remainder. A field emission scanning electron microscope (FESEM) image depicted the microstructure.

References

Al-Husseny, W.H., Al-Sharuee, I.F., & Ali, R. (2022). Water glass based superhydrophobic silica aerogel in different environmental of preparation. *New Materials, Compounds and Applications*, *6*(2), 127-139.

Al-Mothafer, Z., Abdulmajeed, I., & Al-Sharuee, I. (2021). Effect of oxalic acid as a catalyst and dry control chemical additive (dcca) for hydrophilic aerogel base sodium silicate by ambient pressure drying. *Journal of Ovonic Research*, *17*(2), 175-183.

Al-Sharuee, I., Ali, B.R. (2023). Absorption Spectrum and Raman Spectroscopy of Coumarin507 Dye Laser in Different Solvents. *Diffusion Foundations and Materials Applications*, 32, 45-51.

Al-sharuee, I.F. (2019). Thermal conductivity performance of silica aerogel after exposition on different heating under ambient pressure. *Baghdad Science Journal*, *16*(3), 0770-0770.

AL-Sharuee, I.F. (2021). Specifications study of Hydrophobic Silica Aerogel Doped with Rhodamine 6G Prepared via Sub-Critical Drying Technique. *Iraqi Journal of Science*, 483-489.

Berardi, U., Zaidi, S.M. (2019). Characterization of commercial aerogel-enhanced blankets obtained with supercritical drying and of a new ambient pressure drying blanket. *Energy and Buildings*, *198*, 542-552.

Braidotti, M.C., Gentilini, S., Fleming, A., Samuels, M.C., Di Falco, A., & Conti, C. (2016). Optothermal nonlinearity of silica aerogel. *Applied Physics Letters*, *109*(4), 041104.

Cheng, Y., Xia, M., Luo, F., Li, N., Guo, C., & Wei, C. (2016). Effect of surface modification on physical properties of silica aerogels derived from fly ash acid sludge. *Colloids and Surfaces A: Physicochemical and Engineering Aspects*, *490*, 200-206.

Depla, A., Lesthaeghe, D., van Erp, T. S., Aerts, A., Houthoofd, K., Fan, F., Li, C., Van Speybroeck, V., Waroquier, M., & Kirschhock, C. E. (2011). 29Si NMR and UV-Raman investigation of initial oligomerization reaction pathways in acid-catalyzed silica sol-gel chemistry. *The Journal of Physical Chemistry C*, *115*(9), 3562-3571.

Du, A., Zhou, B., Zhang, Z., & Shen, J. (2013). A special material or a new state of matter: a review and reconsideration of the aerogel. *Materials*, *6*(3), 941-968.

Falsafi, M.H., Moghaddas, M., & Moghaddas, J. (2020). Removal of heavy metals from synthetic wastewater using silica aerogel-activated carbon composite by adsorption method. *Journal of Applied Research in Water and Wastewater*, *7*(1), 90-96.

Huang, Y., He, S., Feng, M., Dai, H., Pan, Y., & Cheng, X. (2019). Organic solvent-saving preparation of water glass based aerogel granules under ambient pressure drying. *Journal of Non-Crystalline Solids*, *521*, 119507.

Jathar, L.V., Kulkarni, M., Himatsinghani, D., Ajwani, N., & Achalawat, D.G. (2021). Comparative Study of Coumarin-120 (C-120) and Stilbine-3 (STB-3) Laser Dyes Doped in Sol-Gel Glasses. *New Journal of Glass and Ceramics*, *11*(3), 57-82.

Kottsov, S.Y., Shmelev, M.A., Baranchikov, A.E., Kiskin, M.A., Sharipov, A.U., Efimov, N.N., Rubtsova, I.K., Nikolaevskii, S.A., Kopitsa, G.P., & Khamova, T.V. (2023). Aerogel-Based Single-Ion Magnets: A Case Study of a Cobalt (II) Complex Immobilized in Silica. *Molecules*, *28*(1), 418.

Li, M., Jiang, H., & Xu, D. (2018). Preparation of sponge-reinforced silica aerogels from tetraethoxysilane and methyltrimethoxysilane for oil/water separation. *Materials Research Express*, *5*(4), 045003.

Lovskaya, D., Lebedev, A., & Menshutina, N. (2015). Aerogels as drug delivery systems: In vitro and in vivo evaluations. *The Journal of Supercritical Fluids*, *106*, 115-121.

Martinelli, A. (2014). Effects of a protic ionic liquid on the reaction pathway during non-aqueous sol–gel synthesis of silica: A Raman spectroscopic investigation. *International Journal of Molecular Sciences*, *15*(4), 6488-6503.

Mohammadian, M., Kashi, T.S.J., Erfan, M., & Soorbaghi, F.P. (2018). Synthesis and characterization of silica aerogel as a promising drug carrier system. *Journal of Drug Delivery Science and Technology*, *44*, 205-212.

Quino, J., Ruehl, M., Klima, T., Ruiz, F., Will, S., & Braeuer, A. (2016). Supercritical drying of aerogel: In situ analysis of concentration profiles inside the gel and derivation of the effective binary diffusion coefficient using Raman spectroscopy. *The Journal of Supercritical Fluids*, *108*, 1-12.

Ramirez, N., Zámbó, D., Sardella, F., Kißling, P. A., Schlosser, A., Graf, R. T., Pluta, D., Deiana, C., & Bigall, N. C. (2021). Pd-Doped Cellulose Carbon Aerogels for Energy Storage Applications. *Advanced Materials Interfaces*, *8*(12), 2100310.

Rzhevskii, A. (2021). *Modern Raman Microscopy: Technique and Practice*. Cambridge Scholars Publishing.

Sarawade, P.B., Kim, J.-K., Hilonga, A., & Kim, H.T. (2010). Influence of aging conditions on textural properties of water-glass-based silica aerogels prepared at ambient pressure. *Korean Journal of Chemical Engineering*, *27*, 1301-1309.

Stergar, J., Maver, U. (2016). Review of aerogel-based materials in biomedical applications. *Journal of Sol-Gel Science and Technology*, *77*, 738-752.

Tang, X., Sun, A., Chu, C., Yu, M., Ma, S., Cheng, Y., Guo, J., & Xu, G. (2017). A novel silica nanowire-silica composite aerogels dried at ambient pressure. *Materials & Design*, *115*, 415-421.

Wang, J., Bokhimi, X., Morales, A., Novaro, O., Lopez, T., & Gomez, R. (1999). Aluminum local environment and defects in the crystalline structure of Sol− Gel alumina catalyst. *The Journal of Physical Chemistry B*, *103*(2), 299-303.

Yun, S., Luo, H., & Gao, Y. (2014). Superhydrophobic silica aerogel microspheres from methyltrimethoxysilane: rapid synthesis via ambient pressure drying and excellent absorption properties. *RSC Advances*, *4*(9), 4535-4542.

Zhang, D., Yu, W., Hao, D., Li, L., Liu, H., & Lu, Z. (2012). Functional nanostructured surfaces in hybrid sol–gel glass in large area for antireflective and super-hydrophobic purposes. *Journal of Materials Chemistry*, *22*(33), 17328-17331.